Fabrication and characterization of oxide dispersion strengthened (ODS) 14Cr steels consolidated by means of hot isostatic pressing, hot extrusion and spark plasma sintering

I. Hilger [a,e], X. Boulnat [b,f], J. Hofmann [c], C. Testani [d], F. Bergner [a,*], Y. De Carlan [b], F. Ferraro [d], A. Ulbricht [a]

[a] Helmholtz-Zentrum Dresden-Rossendorf, Bautzner Landstraße 400, 01328 Dresden, Germany

[b] CEA, DEN, Service de Recherches Métallurgiques Appliquées, 91191 Gif-sur-Yvette, France

[c] Karlsruhe Institute of Technology, Institute for Applied Materials, P.O.Box 3640, 76021 Karlsruhe, Germany

[d] Centro Sviluppo Materiali, Castel Romano, Via di Castel Romano 100, 00128 Roma, Italy

[e] Institute of Materials Science, TU Dresden, 01062 Dresden, Germany

[f] Université de Lyon, INSA-Lyon, MATEIS UMR CNRS 5510, 69621 Villeurbanne, France

Abstract: Ferritic ODS 14Cr steels are one of the options for future nuclear and non-nuclear energy applications, in particular for components exposed to higher operation temperatures. In order to better exploit the potential advantages of ODS ferritic steels, such as improved creep strength and damage tolerance (with respect to non-ODS high-chromium steels) along with excellent oxidation resistance, a broader scientific and technical background is required. The present collaborative approach aimed to contribute to this background with respect to both fabrication issues and nano-/microstructurally based understanding of the resulting properties. In particular, the feasibility of ODS steel fabrication by means of spark plasma sintering on a semi-industrial scale was to be demonstrated. Parameter variations related to mechanical alloying, consolidation and thermal/mechanical treatments were covered. Hot extrusion was successfully applied to produce a 2.5 kg batch of ODS steel. Spark plasma sintering was scaled up towards semi-industrial 0.5 kg batches. A set of characterization techniques including Small-Angle Neutron Scattering, Transmission Electron Microscopy, Atom-Probe Tomography, Electron Probe Micro-Analysis, Electron Back-Scatter Diffraction and Transmission Kikuchi Diffraction as well as

* Corresponding author. Tel.: +49 351 260 3186; fax: +49 351 260 2205.
E-mail address: f.bergner@hzdr.de (F. Bergner).

mechanical testing were applied to characterize the materials at different scales and stages of the fabrication process and to underpin the findings, such as a pronounced bimodality of grain size distributions, by observation-based understanding.

KEY WORDS: ODS steel, mechanical alloying, hot extrusion, spark plasma sintering, microstructure, mechanical testing

1 Introduction

High-Chromium oxide-dispersion strengthened (ODS) steels with oxide particles in the low nm-range are candidate materials for future applications in nuclear energy systems [1-4] for both nuclear fission [5] and fusion [6,7]. The key point is a promising combination of properties including favorable resistance against corrosion [8], creep and swelling [5] as well as good irradiation damage tolerance [9]. The standard powder metallurgy (PM) route of fabrication of ODS steels consists of gas atomization of a pre-alloy, mechanical alloying (MA), consolidation and thermal/mechanical treatment. It is expensive in comparison with conventional ingot metallurgy routes; details of the individual steps of the PM route are not yet well understood with the consequence of both scatter and limited reproducibility of the quality of the end product; scaling-up of the process steps towards an industrial scale may pose problems. The challenges required to overcome these drawbacks are addressed in current worldwide research efforts. For instance, advanced techniques of gas atomization lead to an increased efficiency of powder production [10]. A number of parameter studies aim at understanding the roles of composition [11], milling parameters [12], details of the consolidation process and post-processing on the quality in terms of inhomogeneity [12], anisotropy [13], reproducibility and properties [11-14] of the ODS steel. In [11] it was shown that, although Y_2O_3-added alloys display the best performance in terms of tensile behavior, stable oxides other than Y_2O_3 are able to form fine ODS-particles in ferritic steels. The first effort to apply spark plasma sintering to produce ODS Fe-Cr model alloys was reported in [12] indicating a suitable combination of initial powders and parameters of both mechanical alloying and consolidation. Work reported in [13] was focused on the effect of microstructural anisotropy on the mechanical properties of extruded bars of an ODS Fe14Cr-based steel. Alternative fabrication routes including ingot (melting+casting) metallurgy [15] and hybrid techniques [14] have been suggested but are beyond subject of the present investigation.

As conclusion from the literature review and the resulting identification of knowledge gaps it was decided to concentrate on selected subjects within the collaborative research effort. These include variations of the parameters of the MA process, the consideration of the relatively new consolidation process of spark plasma sintering

(SPS) along with the more classic processes of hot isostatic pressing (HIP) and hot extrusion (HE) as well as selected methods of thermal/mechanical treatment including hot rolling (HR) and hot cross rolling (HCR). It was also decided to start from commercially available gas atomized steel powders and yttria powders (except for an individual study, where the powder particle type was varied). In order to reduce the number of variables further, a composition close to Fe-14Cr-1W-0.4Ti was selected, meaning that the work was focused on ferritic ODS steels and the range of possible microstructures was confined with respect to the entire field of ferritic/martensitic ODS steels.

Since each of the individual efforts cannot be fully detailed here, this report is aimed to focus on the following aspects:

- The chain based on MA, consolidation via HIP and HE and treatments by means of HR and HCR was to be realized on an industrial (weight >1000 g) or semi-industrial (weight ~500 g) scale.
- Consolidation by means of SPS was to be optimized on the laboratory scale and to be transferred to the semi-industrial scale.
- Nano- and microstructural techniques as well as mechanical testing were to be adapted and applied to characterize the features required to describe and understand the quality of the fabricated batches of ODS steels.
- Conclusions were to be drawn about the rationalization of the resulting microstructures and about the most promising set of parameters for each fabrication route.

The composition of the materials, the details of the applied PM processes and the characterization techniques will be introduced in the experimental section. The results section will give an overview of some important results achieved in the framework of the project. For further results on selected aspects, we refer to the published literature. Progress achieved by the contributing partners will be elaborated in the discussion section. The conclusions are aimed to highlight new insight.

2 Experiments

2.1 Materials and PM process

Composition

Steel powders produced by means of gas atomization were provided by Aubert&Duval, France, and Nanoval, Germany. In order to reduce the number of degrees of freedom, the nominal composition of the steel powders was specified beforehand to approach the composition Fe-14Cr-1W-0.4Ti-0.3Mn-0.3Si-0.15Ni (wt%). This corresponds to one of the candidate compositions for the application of ODS steels for cladding tubes in future sodium fast reactors [5]. Moreover, a Cr content of 14 wt% guarantees the formation of a fully ferritic microstructure and, therefore, eliminates complications caused by mixed ferritic-martensitic microstructures. The composition of the Nanoval steel powder used by HZDR is specified in Table 1. The yttria nano-powders used by the contributors were produced by Plasma & Ceramic Technologies (PCT) Ltd., Latvia, and in one case by Sigma Aldrich. The same batch of PCT yttria powder was shared by the contributors in order to reduce the number of variables. Amounts of 0, 0.3 or 0.6 wt% Y_2O_3 were added except for one series of trials, where 0.3 wt% La_2O_3, ZrO_2, Ce_2O_3 or MgO were introduced into the powder mixture instead of Y_2O_3 to study the effect of the type of oxide [11].

Table 1 Analysis of one of the gas atomized steel powders (steel2).

Fe (wt%)	Cr (wt%)	W (wt%)	Ti (wt%)	Si (wt%)	Mn (wt%)	Ni (wt%)	C (ppm)	N (ppm)	O (ppm)
bal.	14.1	0.99	0.32	0.18	0.34	0.17	<60	2.7	4.9

Mechanical alloying and consolidation

The blended powders were mechanically alloyed using attritor or planetary ball mills. In selected cases, the milling speed and time were varied systematically in order to study the effect of the milling conditions on the milled powders or compacts. Such a subset of powders milled using a Fritsch Pulverisette 5 planetary ball mill is summarized in Table 2, where the values of yttria content, milling time and milling speed are specified. These powders were later compacted using SPS. Another subset of powders (KIT) was milled using a ZOZ Simoloyer CM01 attritor ball mill operating at 800/1200 rpm (revolutions per minute) for 24, 48 and 80 hours prior to compaction using HIP. Additionally, a larger-scale horizontally rotating low-energy

dry-ball miller manufactured in house at CSM with a capability of about 6 dm^3 was used by one partner. In this case it was possible to charge the jar (with vacuum-proof-device) with more than 2 kg of matrix powders per batch added with 0.3wt% of Y_2O_3. The rotation speed was of about 60-80 round per second (about 3600 rpm) with a jar diameter of about 200 mm that allowed enough energy to promote mechanical alloying. In this case, mixed Ar-H environments have been introduced to reduce oxygen pick-up during the mechanical alloying process. The powder-to-ball weight ratio was 1:10 for all the subsets of powders. An alternative way of introducing the yttrium into the material was evaluated by one partner. Namely, a powder consisting of the intermetallic compound Fe_3Y was added to further reduce the oxygen content of the materials.

Three consolidation methods were employed, namely hot isostatic pressing (HIP), hot extrusion (HE) and spark plasma sintering (SPS). Some focus was put on SPS as an alternative technique capable of reducing the exposure time to high temperatures and, therefore, potentially inhibiting grain growth. Successful applications of SPS were reported before for Fe-based alloys [16,17] and, in particular, for ODS alloys [12,18]. In some cases, the samples for further investigation were taken from the as-consolidated compacts, in other cases, additional hot rolling (HR) or hot cross rolling (HCR) was performed, the latter in order to reduce rolling-induced anisotropy.

An extract of the set of fabricated ODS steels is specified in Table 2. Details on the composition, the mechanical alloying (MA) process (type of mill, atmosphere, milling speed and time), consolidation (type of consolidation, temperature, time, pressure) and thermal/mechanical treatment including HR and HCR are given. HR (Fig. 1) was performed at 1100°C with a thickness reduction from 40 mm (diameter of the as-HIPed compact) to 6 mm (thickness of the rolled plate) in six steps.

For in-depth investigations on selected special aspects, we refer to the literature published during the project phase [11,19-22]. Standard or sub-sized specimens were cut from the pieces of material for mechanical testing. Samples for microstructural analyses were also prepared taking into account types of anisotropy expected in particular for extruded or rolled products.

Fig. 1. Snap-shots of ODS steel fabrication via HIP (left) and HR (middle and right).

Table 2 Selected batches of ODS steels and model alloys fabricated in the framework of the MATTER project.

Batch	Composition * (wt%)	MA speed/time (rpm/h)	Consolidation temperature/time/pressure (°C/min/MPa)	Mass (g)
KIT1	steel1+0.3Y_2O_3	Ar 1000/24	HIP 1150/60/100	~500
KIT2	steel1+0.3Y_2O_3	Ar 1000/48	HIP 1150/60/100	
KIT3	steel1+0.3Y_2O_3	Ar 1000/80	HIP 1150/60/100	
KIT4	steel1+0.3Y_2O_3	Ar 1000/80	HIP 1150/60/100 + HR	
KIT5	steel1+1.3Fe_3Y	Ar 1000/80	HIP 1150/60/100 + HR	
KIT6	steel1+1.3Fe_3Y	Ar 1000/80	HE	~1000
KIT7	steel1 + different types of oxides [11]			
HZD1	steel2, no Y_2O_3	Ar 150/20	SPS 1050/10/70	~20, 200
HZD2	steel2, no Y_2O_3	Ar 250/30	SPS 1050/10/70	
HZD3	steel2, no Y_2O_3	Ar 250/50	SPS 1050/10/70	
HZD4	steel2+0.3Y_2O_3	Ar 150/20	SPS 1050/10/70	
HZD5	steel2+0.6Y_2O_3	Ar 150/20	SPS 1050/10/70	
HZD6	steel2+0.6Y_2O_3	Ar 250/30	SPS 1050/10/70	
HZD7	steel2+0.6Y_2O_3	Ar 250/50	SPS 1050/10/70	
HZD8	Fe-14Cr + 5% Y_2O_3 to observe by means of X-ray diffraction structural changes of Y_2O_3 during milling [22]			
CEA1	steel3+0.3Y_2O_3	**	HIP 1160/180/100	1500
CEA2	steel3+0.3Y_2O_3	**	SPS 850/5/60	15
CEA3	steel3+0.3Y_2O_3	**	SPS 1150/2/60	
CEA4	steel3+0.3Y_2O_3	**	SPS 1150/20/60	
CEA5	steel3+0.3Y_2O_3	**	SPS 1150/200/60	
CEA6	steel3+0.3Y_2O_3	**	SPS 1150/2/76	
CEA7	steel3+0.3Y_2O_3	**	SPS 1150/5/76	450
CEA8	steel3, no Y_2O_3	Ar -/12	SPS 1150/5/76	450
CSM1A	steel2+0.3Y_2O_3	vacuum -/48	HIP 1150/45/125	1000 -3000
CSM1B	steel2+0.3Y_2O_3	vacuum -/48	HIP 1150/45/125 + HCR	
CSM1C	steel2+0.3Y_2O_3	vacuum -/48	HIP 1150/45/125 + HE	
CSM2	steel2+0.3Y_2O_3	vacuum -/80	HE	
CSM3	steel2+0.3Y_2O_3	Ar+H -/100	HE + diff. annealings	

* Powder composition of steel1 (wt%): 13.35 Cr, 0.87 W, 0.21 Ti, 0.18 Si; composition of steel2: see table 1; Composition of steel3 after MA: 14.6 Cr, 0.99 W, 0.32 Ti, 0.19 Si.

** High energy attritor under hydrogen atmosphere (Plansee), 12 hours as trade-off between fragmentation and contamination, batches of 10 to 13 kg.

2.2 Characterization

Microstructure

Along with basic quality control such as porosimetry, the following microstructural characterization techniques were applied to powders and/or compacts according to the needs of the individual subtasks of the project:

- optical microscopy (OM),
- scanning electron microscopy (SEM) also in combination with energy dispersive X-ray spectroscopy (EDX) and electron back-scatter diffraction (EBSD) or transmission Kikuchi diffraction (TKD),
- electron probe microanalysis (EPMA) on powder fills and compacts,
- transmission electron microscopy (TEM),
- atom probe tomography (APT),
- small-angle neutron scattering (SANS) on as-milled powder, shown to be applicable before [23], and on compacts.

These techniques are comparatively well known except for TKD [24], which is a transmission version of EBSD (Fig. 2). Using a SEM equipped with TKD, higher resolution than known from EBSD can be achieved, which means that smaller grains can be visualized, an essential feature in the field of advanced ODS steels.

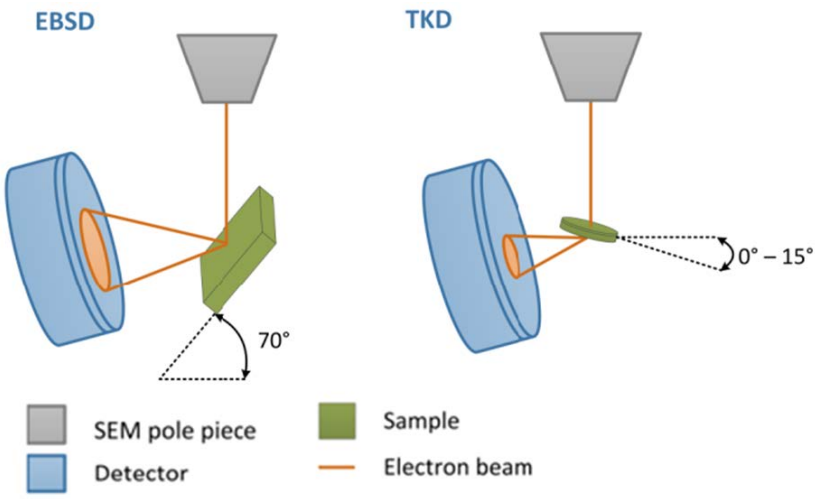

Fig. 2. Path of electron beam and sample in EBSD and TKD.

Mechanical properties

In order to estimate the mechanical properties of the materials listed in Table 2, nanoindentation, Vickers hardness, tensile testing and impact testing using standard or sub-sized specimens, according to the volumes of material available, were performed. It is important to note that the aim of mechanical testing was to explore the role of fabrication parameters within each subset of materials. Any ranking from subset to subset or from manufacturer to manufacturer was beyond the scope of the project.

3 Results

Batches KIT1-KIT6

In the first phase of the project experiments focused on standard 13Cr-ODS alloys were carried out (KIT1-3). Based on an already existing set of parameters, the milling time was varied and experimentally validated by means of microtomy and TEM examinations of the mechanically alloyed powders [19]. The milled powders were then exposed to HIP, HIP+HR and HE.

Impact tests were performed using V-notched KLST specimens of dimensions 3 x 4 x 27 mm^3 and L-T orientation. The resulting temperature dependence of the impact energy is compared in Fig. 3 for as-HIPed, HIPed+rolled and as-extruded materials. It is found that the behavior of the as-extruded material is favorable in the present case.

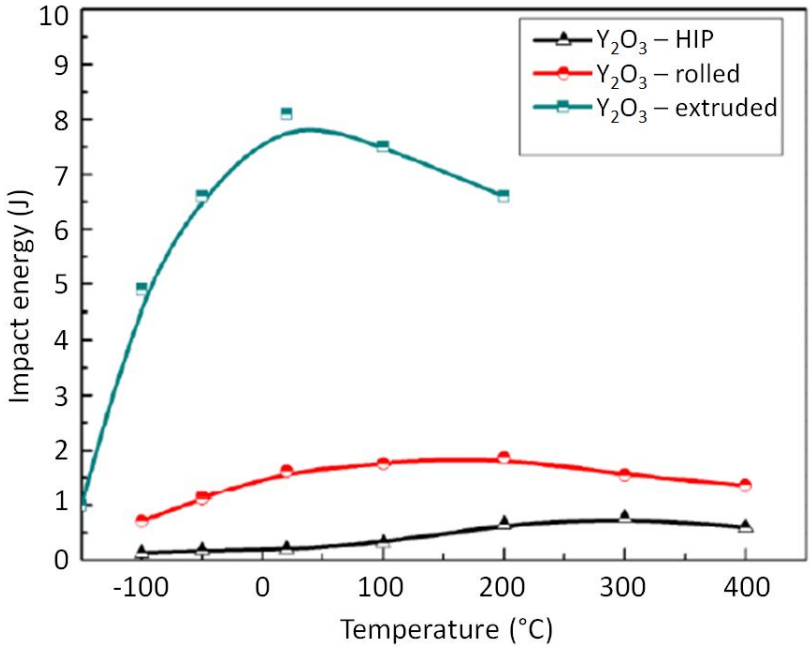

Fig. 3. Temperature dependence of impact energy for 13Cr ODS steels consolidated via HIP, HIP+HR and HE.

For the results obtained for batches KIT7 covering varying types of oxides, we refer to [11]. It is demonstrated that stable oxides other than Y_2O_3 are able to form fine ODS-particles in ferritic steels.

Batches HZD1-HZD7

The variation of yttria contents and milling parameters performed for batches HZD1-HZD7 resulted in different microstructures. Most interestingly, a distribution of oxide particles in the low-nm range was observed by means of SANS (powders and compacts) and APT (compacts) not only for the Y_2O_3 containing materials but also for Y-free materials. This is clearly seen in the SANS results in Fig. 4 obtained for milled powders. The difference scattering curves displayed in Fig. 4(a) were obtained by subtracting the lower-bound Q^{-4} dependence of the measured magnetic scattering cross section from the cross section itself. In this way, the scattering caused by nm-scale particles is separated from the background caused by scattering at coarser microstructural features. The fitted curves in Fig. 4(a) represent, as an indicator of the goodness of fit, the Fourier transforms of the reconstructed size distributions in Fig. 4(b). Fig. 4(b) shows that the total volume fraction of nanoparticles, i.e. the area under the curves, for Y-free powder is almost as high as for the powder milled after Y_2O_3 addition. Further SANS experiments on SPS-compacted samples reported elsewhere indicate that the total volume fraction of nanoparticles in the Y-free

compact does not increase with respect to the powder, whereas there is a dramatic increase for the compacted Y_2O_3-containing powder for a milling speed of 250 rpm (but not for 150 rpm).

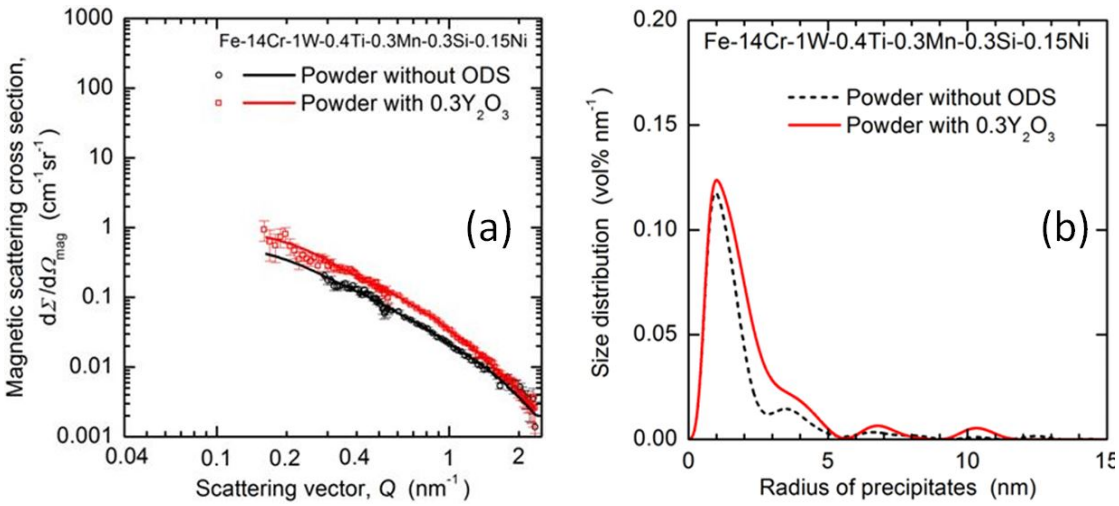

Fig. 4. Magnetic difference scattering curves (a) and reconstructed size distribution of oxide particles (b).

EBSD and TKD measurements revealed pronounced bimodalities of the grain size distributions for all SPS compacts, both HZDx and CEAx. Fig. 5 displays a TKD inverse pole figure map (right subfigure) recorded in the ultrafine-grained area marked in the color-coded ARGUS image (left subfigure). It is interesting to note that, using conventional EBSD, it was impossible to resolve the grains in the ultrafine-grained region.

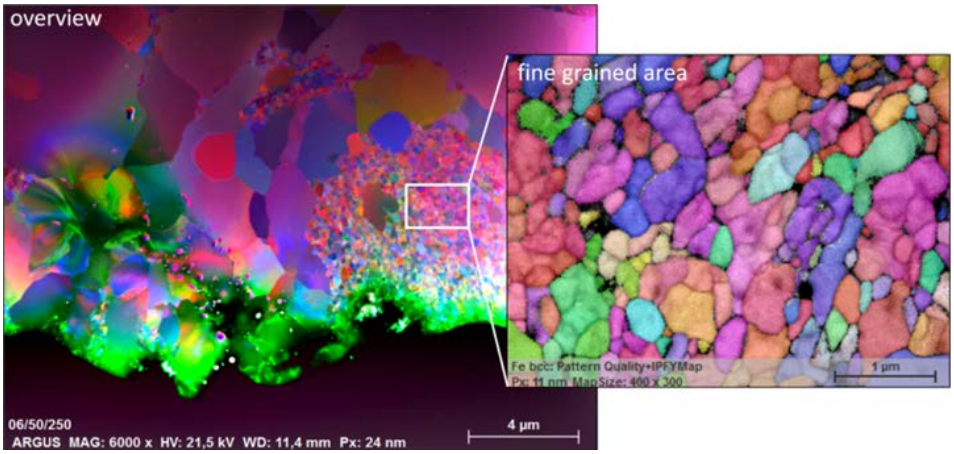

Fig. 5. TKD image of a SPS-compacted sample taken from batch HZD7.

Scanning nanoindentation (Fig. 6) indicates that homogeneity of the SPS compact is poor on the µm scale after 20h/150rpm of MA. The hardness variations decrease significantly towards 30 h/250 rpm and then marginally towards 50 h/250 rpm. However, the homogeneity is still poor compared to ODS 14Cr bar extruded at 1100 °C (extrusion ratio 10) followed by annealing at 1050 °C/1.5 h [5,13] shown for comparison. MA of the powder for extrusion was performed in a vertical attritor under hydrogen atmosphere.

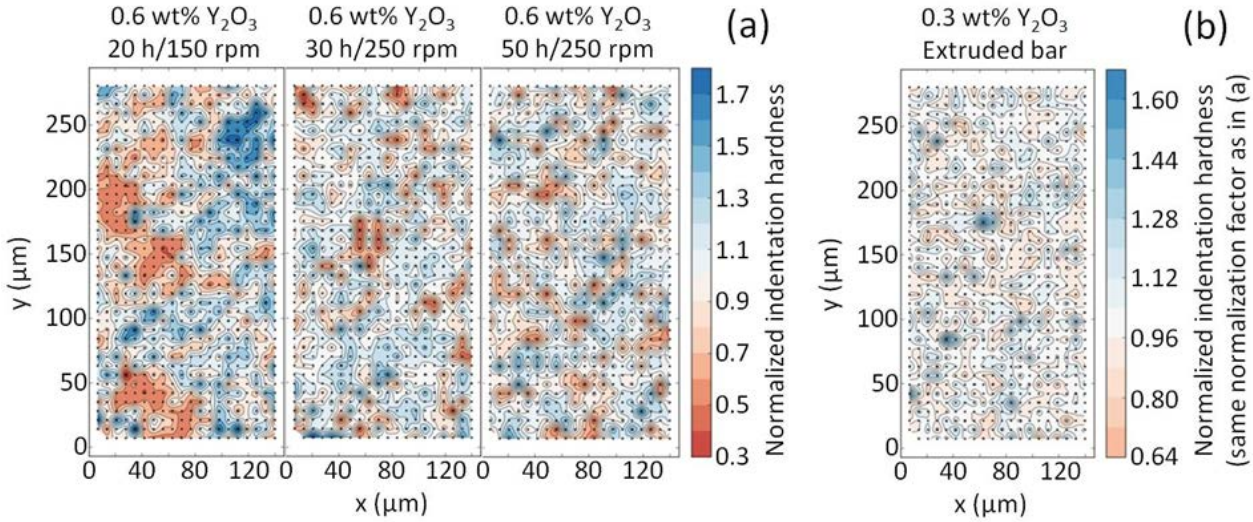

Fig. 6. Scanning nanoindentation applied to characterize spatial hardness variations on the 10 µm scale, (a) SPS compacts of the present work, (b) extruded bar material from previous work [5,13].

Batches CSM1-CSM3

The industrial-scale batches CSM1 and CSM2 were produced successfully by means of HIP (1A), HE (2) as well as of combinations of HIP + HCR (1B) and HIP + HE (1C), see table 2. However, hardness measurements indicated that these batches did not reach the anticipated levels of hardness. Therefore, the milling parameters (atmosphere and milling time) were once more modified to reach higher hardness.

Mechanically alloyed CSM samples were characterized by means of TEM. The typical microstructure is reported in Fig. 7(a). The grain size distribution was found to be bimodal with larger grains of dimension of about 1-2 µm and smaller grains of size smaller than 0.5 µm. An example of in-situ precipitated nm-sized particles is given in Fig. 7(b). The EDX analysis of a single particle shown in Fig. 8 reveals a complex structure of a Y-Si-Ti oxide.

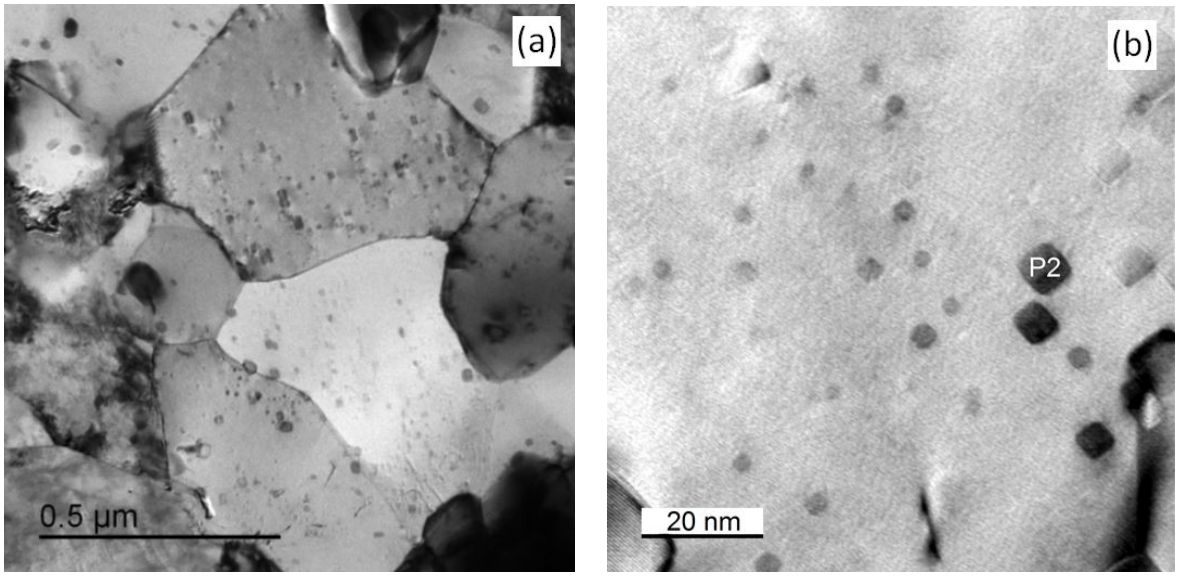

Fig. 7. TEM images of microstructure (a) and nano-precipitates (b) in sample CSM3.

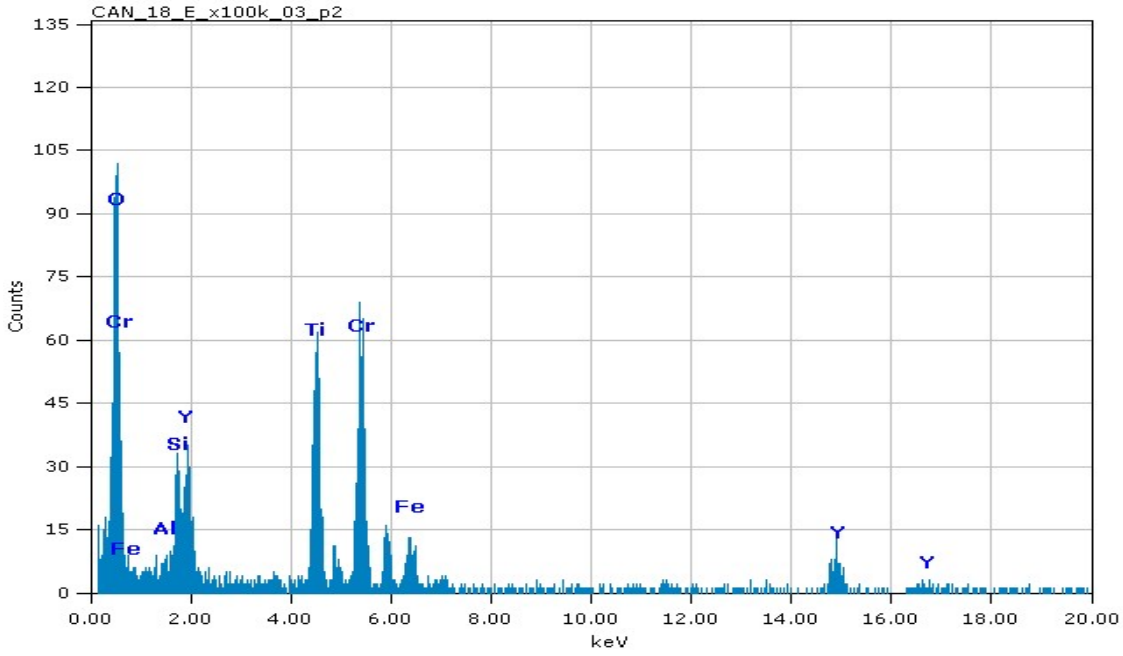

Fig. 8. Complex diffraction spectrum of particle P2 in Fig. 7.

The hot extruded batch CSM3 was then exposed to annealing treatments and tensile tests in the temperature range from RT to 800°C. The tensile test results are summarized in Fig. 9, where they are compared with data obtained for a stainless steel tested under identical conditions. 70 mm long tensile round bars according to ASTM E8, one per temperature, were tested for each material.

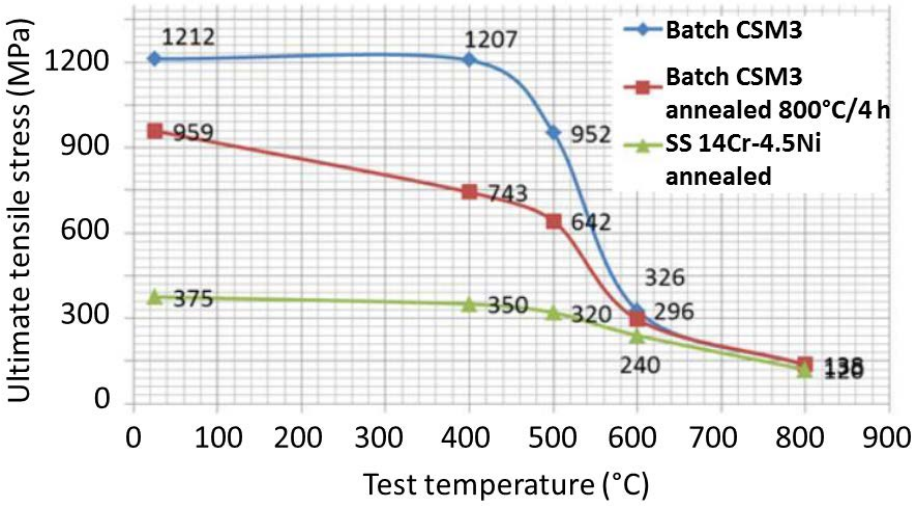

Fig. 9. Ultimate tensile stress as function of test temperature for as-extruded and extruded and annealed material.

The ultimate tensile stress of about 1200 MPa at 400°C obtained for a more than 2.5 m long extruded bar of ferritic Fe-14Cr ODS steel with a weight of about 2.5 kg is an encouraging result under the aspect of industrial scale ODS steel fabrication. Moreover such results have been obtained on standard ASTM E8 specimens, not on sub-sized specimens.

Batches CEA1-CEA8

The composition of the mechanically alloyed powder and a compacted sample obtained by means of EPMA is summarized in Table 3. Given the composition of the initial steel powder according to the nominal composition of Fe-14Cr-1W-0.4Ti-0.3Mn-0.3Si-0.15Ni (wt%) and similar to the analysis in Table 1 as well as the yttria addition, this is a reasonable result. Worth noticing is that oxygen content did not significantly increase with consolidation.

Table 3 Mean composition (wt%) of the MA powder and the SPS-consolidated sample (1150 °C) measured by means of EPMA (balance Fe).

Element	Cr	W	Y	O	Ti	Si
Powder	14.6±0.1	0.99±0.02	0.16±0.02	0.15±0.01	0.32±0.02	0.19±0.01
Compact	14.5±0.1	1.01±0.02	0.16±0.02	0.15±0.06	0.32±0.03	0.18±0.01

The powders were compacted by means of SPS using the parameters given in Table 2 and using heating rates of 500 K/min and cooling rates of 200 K/min for batches CEA2 to CEA6. Sample CEA7 with slightly lower heating rate of 300K/min was tested for scaling-up the process [25]. The measured relative densities are listed in Table 4 in terms of percent of the theoretical density.

Table 4 Measured relative density after SPS consolidation using different process parameters.

Batch	CEA2	CEA3	CEA4	CEA5	CEA6	CEA7	CEA8
Relative density (%)	84±1	95±1	97±1	98±1	99±1	98±1	99±1

As mentioned above, a pronounced bimodality of the grain size distributions was also observed for the samples from batches CEA2 to CEA7 (Fig. 10) consolidated by means of SPS. Based on the calculation of the stored energy at each step of the consolidation process, the appearance of this structure was explained by the initial heterogeneous spatial distribution of stored energy due to high-energy attrition of the MA powder [21]. The plastic work due to milling can be the cause of the so-called abnormal growth. The heterogeneous microstructure is then stabilized by the nano-precipitation described above.

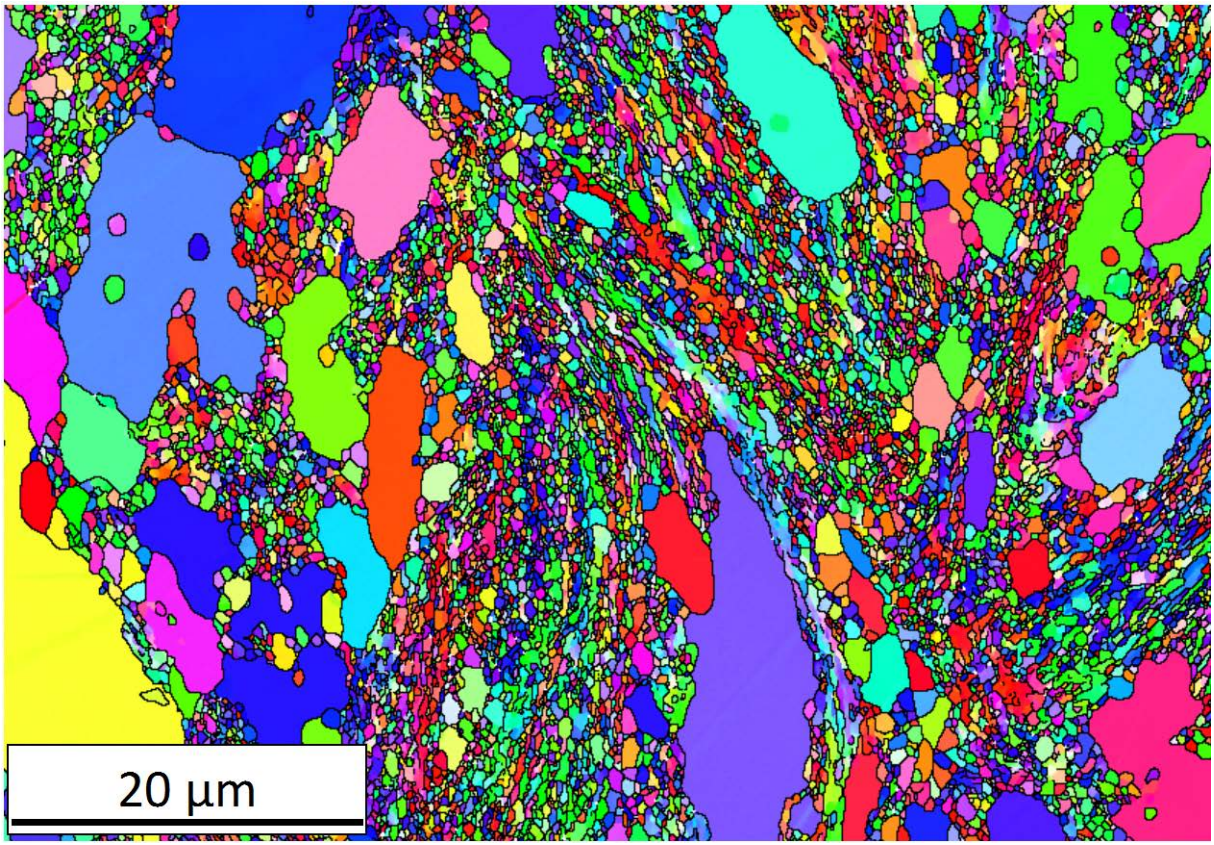

Fig. 10. EBSD map of the bimodal microstructure obtained on CEA7.

In order to investigate the stability of oxide nanoparticles, samples taken from batches CEA1 (HIP) and CEA7 (medium scale SPS) were exposed to annealing treatments at 1100°C for 1 h and 16 h each. SANS was applied to derive the size distribution of oxide nanoparticles in samples consolidated by means of HIP (CEA1) and SPS (CEA7). Scattering curves obtained for samples consolidated from powders without yttria addition (CEA8) were taken as reference (Fig. 11). The results are summarized in Table 5. It is important to note that the yttria-free samples may also contain nanoparticles as shown in Fig. 4 above. Therefore, the data in Table 5 characterize only the population of those oxide nanoparticles formed due to the addition of yttria powder. The A ratio of SANS (A=1+M/N, where M and N are magnetic and nuclear scattering intensity, respectively) of 2.3 is in agreement with the assumption of Ti-containing Y-Ti-O nanoparticles but not with Ti-free yttria [26].

The volume fraction is slightly higher than the value expected from the amount of added yttrium and does not show an obvious trend. The mean radius increases significantly as a function of annealing time, but only for the SPS samples.

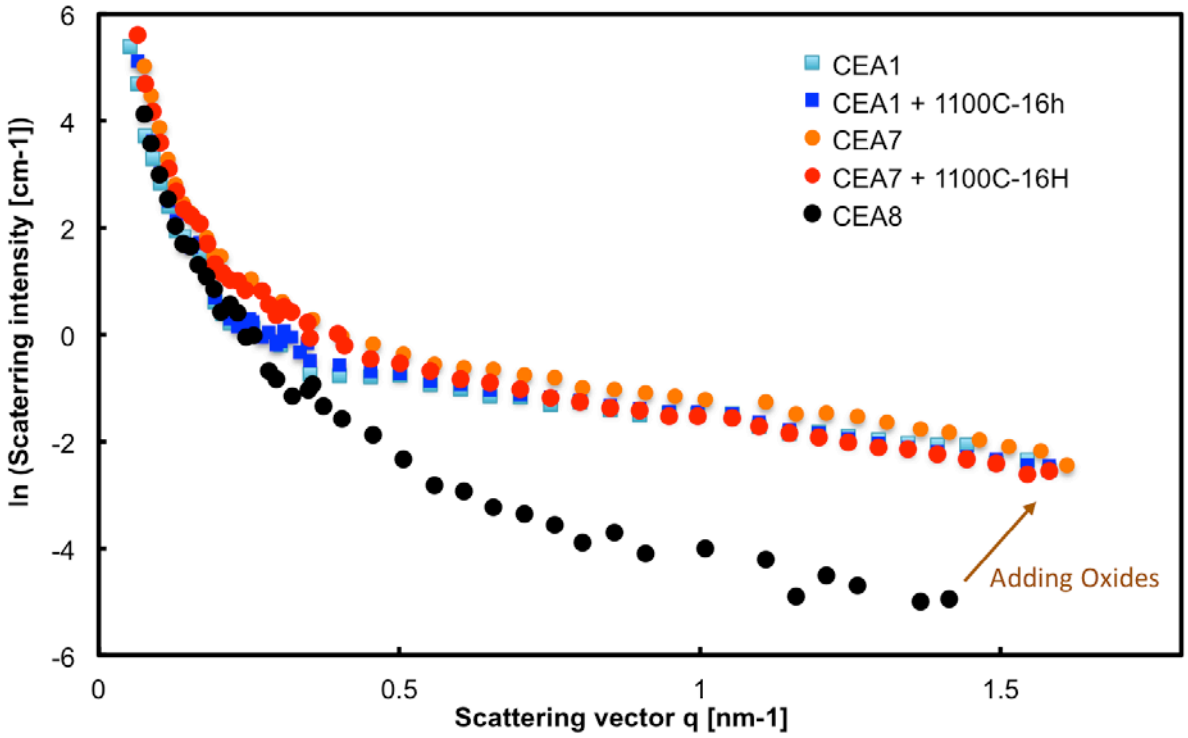

Fig. 11. Scattering intensity of samples with and without oxides after SPS consolidation.

Table 5 Mean radius, r_m, and volume fraction, f_V, of oxide nanoparticles as function of consolidation process and annealing time at 1100°C.

Batch/consolidation	Annealing time (h)	r_m (nm)	f_V (%)
CEA1/HIP	0	1.6	1.1±0.2
	1	1.6	1.0±0.2
	16	1.6	1.1±0.2
CEA7/SPS	0	1.4	1.5±0.4
	1	1.6	1.0±0.2
	16	1.8	1.0±0.2

A summary of high-temperature yield strengths of ODS steels produced by SPS is given in Fig. 12. It is found that the ODS material consolidated at 1150 °C exhibits a reasonable trade-off between strength and ductility. For the full tensile behavior at high temperatures, we refer to [20].

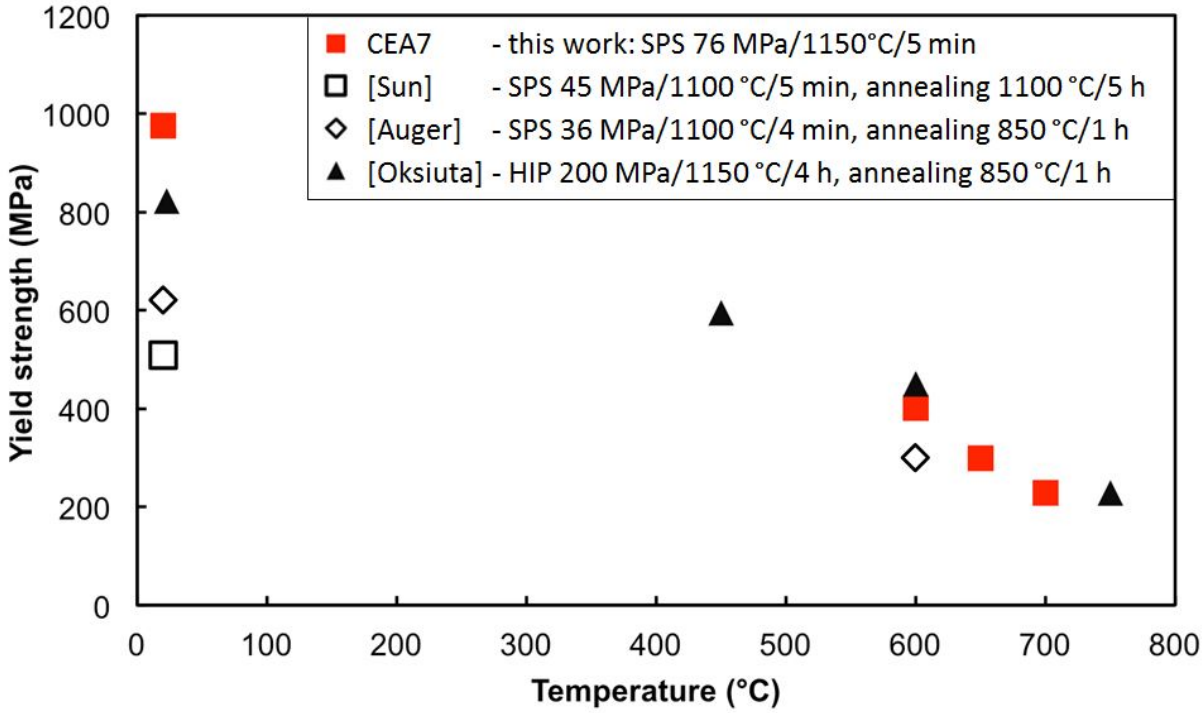

Fig. 12. Room- and high-temperature yield strengths of ODS steels produced by SPS and HIP (references [Sun, Auger, Oksiuta] correspond to [27-29]).

4 Discussion

The present investigation covered several technological steps of the powder metallurgy route towards ODS steels including mechanical alloying, consolidation and thermal/mechanical treatment. The common starting point was commercial gas atomized steel powders of similar nominal compositions of the type Fe-14Cr-1W-0.4Ti-0.3Mn-0.3Si-0.15Ni (wt%) and commercial yttria powder.

The MA parameters were systematically varied within particular parts of the study or fixed according to former experience within other parts, the latter in order to reduce the number of parameters. Variations of the MA parameters in terms of milling time confirmed that there is a trade-off between optimum powder characteristics and oxygen entry. It has been observed on the basis of batch HZD8 that the Y_2O_3 is fragmented and becomes partially amorphous upon milling due to the grain refinement of Y_2O_3 during the milling process [22]. This ultrafine distribution can be considered as the starting situation for the formation of complex nm-sized Y-Ti-O nanoparticles upon consolidation as documented in Table 5. It was shown on the

basis of batch KIT6 that replacement of Y_2O_3 by other types of nano-powders is a future option [11].

Three techniques of powder consolidation were covered in the study, these are HIP, HE and SPS. Each of these techniques was successfully applied, after MA and proper selection of consolidation parameters, to produce dense compacts with relative densities of typically 98% or better. The application of SANS, TEM and APT indicated oxide nanoparticle characteristics that are sufficiently uniform with respect to the spatial distribution (Fig. 7) and near optimum [4] with respect to the size distribution in the low-nm range (Table 5) and the resulting effect on hardening. The application of EBSD, TKD and TEM showed that the grain size distributions exhibit a pronounced bimodality in particular in the case of SPS consolidation (Fig. 5). Bimodal grain size distributions were also reported in other studies on SPS consolidated ODS Fe-Cr based alloys, e.g. [30,31]. It is not yet clear, if bimodality is an inherent feature of this consolidation technique or rather a consequence of MA. Occasionally, bimodality was also reported for other consolidation techniques such as HIP [21,32]. A rationalization of bimodal grain size distributions based on the consideration of abnormal grain growth is reported in [33], to which the present study contributed. The question, under which conditions bimodal grain size distributions are advantageous [30], may depend on application and, in any case, poses a future challenge. An important outcome of the present study was the successful scaling-up of SPS consolidation from the lab scale (weights of 15 and 20 g) towards a semi-industrial scale of 200 and 450 g, e.g. [25]. Similarly, a 2.5 kg batch of hot extruded bar with superior mechanical properties (Fig. 9) was produced.

Hot rolling (from 40 to 6 mm thickness) and hot cross rolling of HIP compacts were applied successfully. While hot rolling is known to produce elongated grains, rolling textures and anisotropic properties, hot cross rolling bears the potential to reduce in-plane anisotropy. Any optimization of thermal, mechanical and thermo-mechanical treatments with respect to the final properties was, however, beyond the scope of the present study.

A broad spectrum of micro- and nanostructural characterization techniques was applied. A fairly complete characterization including composition mapping, grain

structure, texture and distribution of nm-scale particles was achieved in selected cases. Recent technical developments such as TKD and scanning nanoindentation were introduced into the study. Application of TKD allows resolving grain sizes up to a lower limit of about 50 nm. Scanning nanoindentation allows automated mapping of hardness at the mesoscale with µm-scale resolution. Mesoscale spatial homogeneity with respect to hardness (Fig. 6) was introduced as a quality criterion, e.g. for the purpose of optimization of PM process parameters.

Microstructurally based rationalizations of heterogeneous nucleation, grain boundary pinning [21] and hardening mechanisms were proposed.

Mechanical testing performed so far was focused on hardness measurements, tensile tests in a broad range of temperatures and impact testing. Tensile testing revealed superior strength at elevated temperatures, e.g. Figs. 9 and 12 and [21]. In particular, a 2.5 kg batch of hot extruded bar exhibited an ultimate tensile strength of about 1200 MPa between room temperature and 400°C. After an annealing treatment at 800°C for 4 hours, values larger than 700 MPa up to 400°C were maintained indicating a high stability of the oxide nanoparticles shown in Fig. 7(b). These nanoparticles are responsible for the thermal stability of the ultrafine grained zone, which also account for the tensile strength of ODS steels. A drastic decrease of strengths was, however, observed at temperatures higher than 500°C. This indicates a competition in plasticity mechanisms, as suggested in [34].

Impact testing indicated minor increases of the absorbed energy of HIP samples after hot rolling, whereas hot extrusion gives rise to substantially higher values of the absorbed energy (Fig. 3).For follow-up activities, a parameter pre-selection according to the specifications of batches KIT4, CEA7 and CSM3 in Table 2 can be suggested for the semi-industrial consolidation by means of HIP, SPS and HE, respectively. In the case of MA using a planetary ball mill, the milling parameters according to the specification of batch HZD7 (Table 2) were shown to be favorable. Small punch testing and fracture mechanics testing of samples taken from selected batches of the present study are in progress.

5 Summary and conclusions

The joint effort was successful in identifying and combining European resources in the fields of fabrication and characterization of ODS Cr steels for nuclear applications. The work was focused on MA, consolidation by means of HIP, HE and SPS as well as thermal/mechanical treatment of ferritic 14Cr-1W-0.4 Ti with typically 0.3 wt% Y_2O_3 addition. The transfer from laboratory scales towards more industrial scales was also within the scope.

A number of results can be summarized as highlighted below:

- ODS 14Cr-1W-0.4Ti steels were fabricated via different combinations of MA, consolidation and thermal/mechanical treatment.
- One lab succeeded to produce batches of about 2.5 kg weight with an ultimate tensile stress of about 1200 MPa up to 400°C.
- The consolidation technique of SPS was scaled up to weights of 0.2 to 0.5 kg.
- Superior oxide nanoparticle sizes in the low nm-range were identified by means of SANS, TEM and APT.
- Nanostructured aggregates of grains were observed by means of EBSD/TKD and TEM. In some cases, in particular after SPS consolidation, bimodal grain size distributions were found.
- It was possible to rationalize special features such as abnormal grain growth and hardening in terms of nanofeature-based models.

One major insight is that the microstructures of ODS ferritic steels do not strongly depend upon the process used to consolidate the powder. Most of ODS ferritic steels exhibit abnormal structures, even after very short consolidation cycles using SPS. The relatively poor kinetic effect can be explained as follows:

- The strong pinning effect of nano-sized particles is efficient on ultrafine grained zones, in a large range of consolidation temperatures and times.
- Specific grain boundaries exhibit an extremely high mobility that may induce drastic growth of some grains at the expense of the others, most likely in a very short time. This was recently illustrated by in situ synchrotron X-Ray diffraction on selected ODS ferritic steels [33,35].

Another insight is that the initial nanostructure obtained after mechanical alloying plays a major role on the microstructural behavior during high-temperature consolidation. This nanostructure can contain various levels of heterogeneities, including local plastic deformation, as well as local variation of solute compositions [22]. A clean and efficient milling process is a necessary condition to achieve homogeneous and reproducible microstructures of ODS ferritic steels.

Special aspects such as fracture mechanics testing are addressed in ongoing work. Moreover, an industrial-scale effort of ODS-steel fabrication by means of HE based on the alloy composition and consolidation parameters specified for batch CSM3 has been undertaken in the meantime. This will allow reproducibility of the fabrication process, homogeneity at different length scales, mechanical properties, the effect of thermal or thermomechanical treatments, and the irradiation behavior to be investigated in more detail.

Acknowledgement

The MATTER project received funding from the European Commission within the 7th Framework Programme under grant agreement number 269706. This work also contributes to the Joint Programme on Nuclear Materials (JPNM) of the European Energy Research Alliance (EERA). SPS was performed at and in collaboration with the Fraunhofer-Institute IFAM Dresden and the Université de Lyon, INSA-Lyon, MATEIS UMR CNRS. We would like to thank T. Weißgärber (Dresden) as well as M. Perez and D. Fabrègue (Lyon) for granting access to large-scale equipment for the project purposes and for continuing interest. The resourcing of yttria powder by N. De Wispelaere is also gratefully acknowledged.

References

[1] L.K. Mansur, A.F. Rowcliffe, R.K. Nanstad, S.J. Zinkle, W.R. Corwin, R.E. Stoller, J. Nucl. Mater. 329–333 (2004) 166–172.

[2] R.L. Klueh, J.P. Shingledecker, R.W. Swindeman, D.T. Hoelzer, J. Nucl. Mater. 341 (2005) 103–114.
[3] A. Möslang, T. Wiss, Nature Materials 5 (2006) 679–680.
[4] S. Ukai, M. Fujiwara, J. Nucl. Mater. 307–311 (2002) 749–757.
[5] P. Dubuisson, Y. de Carlan, V. Garat, M. Blat, J. Nucl. Mater. 428 (2012) 6–12.
[6] R. Lindau, A. Möslang, M. Schirra, P. Schlossmacher, M. Klimenkov, J. Nucl. Mater. 307–311 (2002) 769–772.
[7] N. Baluc et al., J. Nucl. Mater. 417 (2011) 149–153.
[8] B.V. Mahesh, R.K. Singh Raman, C.C. Koch, Metall. Mater. Trans. 46A (2015) 1814–1824.
[9] J. Brodrick, D.J. Hepburn, G.J. Ackland, J. Nucl. Mater. 445 (2014) 291–297.
[10] A. Allimant, M.P. Planche, Y. Bailly, L. Dembinski, C. Coddet, Powder Technology 190 (2009) 79–83.
[11] J. Hoffmann, M. Rieth, R. Lindau, M. Klimenkov, A. Möslang, H.R. Zschommler Sandim, J. Nucl. Mater. 442 (2013) 444–448.
[12] P. Franke, F. Bergner, C. Heintze, T. Weißgärber, Mechanical Testing 52 (2010) 133–138.
[13] M. Serrano, M. Hernández-Mayoral, A. García-Junceda, J. Nucl. Mater. 428 (2012) 103–109.
[14] J.R. Rieken, I.E. Anderson, M.J. Kramer, G.R. Odette, E. Stergar, E. Haney, J. Nucl. Mater. 428 (2012) 65–75.
[15] K. Verhiest, A. Almazouzi, N. De Wispelaere, R. Petrov, S. Claessens, J. Nucl. Mater. 385 (2009) 308–311.
[16] T. Grosdidier, G. Jia, S. Launois, Scripta Mater. 57 (2007) 525–528.
[17] B. Srinivasarao, K. Oh-ishi, T. Ohkubo, K. Hono, Acta Mater. 57 (2009) 3277–3286.
[18] C. Heintze, M. Hernández-Mayoral, A. Ulbricht, F. Bergner, A. Shariq, T. Weissgärber, H. Frielinghaus, J. Nucl. Mater. 428 (2012) 139–146.
[19] J. Hoffmann, M. Klimenkov, R. Lindau, M. Rieth, J. Nucl. Mater. 428 (2012) 165–169.
[20] X. Boulnat, D. Fabregue, M. Perez, M.-H. Mathon, Y. Decarlan, Metall. Mater. Trans A 44A (2013) 2461–2465.
[21] X. Boulnat, M. Perez, D. Fabregue, T. Douillard, M.-H. Mathon, Y. Decarlan, Metall. Mater. Trans A 45A (2014) 1485–1497.

[22] I. Hilger, M. Tegel, M.J. Gorley, P.S. Grant, T. Weißgärber, B. Kieback, J. Nucl. Mater. 447 (2014) 242–247.
[23] M. Ratti, D. Leuvrey, M.H. Mathon, Y. de Carlan, J. Nucl. Mater. 386–388 (2009) 540–543.
[24] P.W. Trimby et al., Acta Mater. 62 (2014) 69–80.
[25] X. Boulnat, D. Fabregue, M. Perez, S. Urvoy, D. Hamon, Y. de Carlan, Powder Metallurgy 57 (2014) 204–211.
[26] M.H. Mathon, M. Perrut, S.Y. Zhong, Y. de Carlan, J. Nucl. Mater. 428 (2012) 147–153.
[27] Q.X. Sun, T. Zhang, X.P. Wang, Q.F. Fang, T. Hao, C.S. Liu, J. Nucl. Mater. 424 (2012) 279–284.
[28] M.A. Auger, V. de Castro, T. Leguey, A. Muñoz, R. Pareja, J. Nucl. Mater. 436 (2013) 68–75.
[29] Z. Oksiuta, P. Mueller, P. Spätig, N. Baluc, J. Nucl. Mater. 412 (2011) 221–226.
[30] Z. Dapeng, L. Yong, L. Feng, W. Yuren, Z. Liujie, D. Yuhai, Mater. Lett. 65 (2011) 1672-1674.
[31] Y.Q. Wu, K.N. Allahar, J. Burns, B. Jaques, I. Charit, D.P. Butt, J.I. Cole, Cryst. Res. Technol. 49 (2014) 645–652.
[32] M.A. Auger, T. Leguey, A. Muñoz, M.A. Monge, V. de Castro, P. Fernández, G. Garcés, R. Pareja, J. Nucl. Mater. 417 (2011) 213–216.
[33] N. Sallez, X. Boulnat, A. Borbely, J.L. Bechade, D. Fabregue, M. Perez, Y. de Carlan, L. Hennet, C. Mocuta, D. Thiaudiere, Y. Brechet, Acta Mater. 87 (2015) 377–389.
[34] Y. Sugino, S. Ukai, B. Leng, N. Oono, S. Hayashi, T. Kaito, S. Ohtsuka, J. Nucl. Mater. 452, (2014) 628–632.
[35] X. Boulnat , N. Sallez, M. Dadé, A. Borbély, J.-L. Béchade, Y. de Carlan, J. Malaplate, Y. Bréchet, F. de Geuser, A. Deschamps, P. Donnadieu, D. Fabrègue, M. Perez, Acta Mater. 97 (2015) 124–130.